MEMS Aerodynamic Control Surfaces for Millimeter-Scale Rockets

Brian G. Kilberg*, Daniel S. Contreras*, Joseph Greenspun*, Kristofer S. J. Pister*
*Berkeley Sensor and Actuator Center
University of California-Berkeley
Berkeley, California 94720
Email: bkilberg@berkeley.edu

***Abstract*—This work describes the design, fabrication, and assembly of a MEMS aerodynamic control surface for use in millimeter-scale rockets and other miniature aerial vehicles (MAVs). Aerial vehicles of this scale require very small and light control surfaces to operate effectively. We designed MEMS aerodynamic control surfaces using electrostatic inchworm motors and planar silicon pin-joints. These were fabricated in a silicon-on-insulator (SOI) process. The fully assembled fin structure demonstrated maximum torque outputs of 1.6 μNm which is enough to maintain an aerodynamic lift force of 1.4 mN.**

I. Introduction

Rocketry has been a highly effective technology for rapid transportation over large distances, especially in space exploration and space transportation. Currently, most useful rocketry technology is far from portable and is firmly limited to the macroscale. Increases in portability from scaling down rocketry to millimeter-scales could prove to be useful. For example, portable millimeter-scale rockets could be used to deploy large wireless sensor networks quickly and accurately from a single host vehicle, enabling the ability to gather information from a large target area. This could be very useful for time-sensitive situations like search and rescue, and military operations. Militaries are concerned about swarm attacks from low-cost micro air vehicles [1], which will lead to a need for smaller cheaper anti-MAV missiles, perhaps stopping short of the nano-scale predicted by Stephenson [2].

Effective millimeter-scale rocket motors have already been developed. For example, Lindsay et al. demonstrated a dime-sized rocket motor that was capable of short flights [3]. Kovac et al. developed 3-6 mm diameter rocket motors with specific impulse of 100 seconds and burn times of up to 40 seconds [4]. These motors could provide a millimeter-scale rocket with up to 800 meters of range within Earth's atmosphere. However, miniature control surfaces at this scale are requried for further development of feasible millimeter-scale rockets. These control surfaces would require actuators with microscale features.

Miniature control surfaces would also be an enabling technology for pico air vehicles, which are unmanned aerial vehicles (UAVs) that are smaller than 5 cm in any dimension and lighter than 500 mg [5]. By combining recent advances in electrohydrodynamic (EHD) thrust with MEMS aerodynamic control surfaces, we hope to develop centimeter-scale EHD-propelled pico air vehicles in parallel with millimeter-scale rockets [6].

Fortunately, developments in micro-electromechanical systems (MEMS) technologies have made microscale actuators and miniature control surfaces possible. For example, Ho et al. were able to demonstrate aerodynamic control of a meter-scale delta wing by using an array of MEMS actuators to manipulate the flow separation at the leading edge of the wing [7]. Murthy and Krishna also developed pneumatically-actuated microballoon actuators for similar flow separation use [8]. Lyshevski further demonstrated the use of MEMS actuator arrays for control surfaces by designing a smart MEMS array that could modify the surface geometry of a wing into a control surface [9]. Additionally, Low et al. demonstrated the trajectory control of a hypersonic projectile by using pressure-actuated MEMS diaphragms [10].

We propose a MEMS control surface that utilizes electrostatic inchworm motors to rotate a thin silicon fin. Electrostatic inchworm motors are one class of linear MEMS actuators that have a favorable tradeoff between force density and displacement [11], [12]. These motors rely on two sets of electrostatic gap closers that actuate out of phase of each other. Each phase of actuation produces a few microns of displacement, but as these actuators repeatedly operate, these small steps add up to a large displacement. Inchworm motors can be fabricated using lithographic techniques widely used in MEMS fabrication processes. While these motors have been used to actuate microrobots [13] [14], they have yet to be applied to microactuated aerodynamic control surfaces. Additionally, planar silicon-on-insulator (SOI) pin joints [15] can be used to design mechanisms that translate linear inchworm actuation to more complicated motions like rotation [13], which is required for the aerodynamic control surface.

In this work, we describe the design, fabrication, and characterization of this MEMS control surface. We fabricated these devices in a straightforward two-mask SOI process. To assemble the fin structure, we inserted the out-of-plane silicon fin into the SOI device and wirebonded the inchworm drive pads to external solder pads. Finally, we characterized the output force and torque of the fully-assembled fin device.

II. Analysis and Design of MEMS Control Surface

In order to design viable MEMS control surfaces, we first determined the amount of force required to maneuver a millimeter-scale rocket with control surfaces. We then used this force estimate to determine the required fin area and actuator

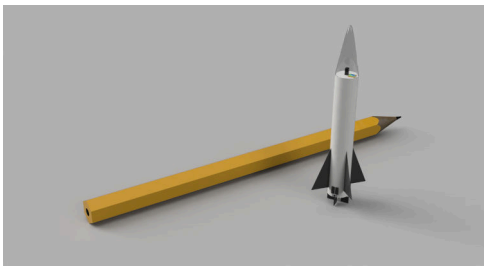

Fig. 1. 3D rendering of proposed millimeter-scale rocket. We generated this rendering using 3D modelling software.

torque for the control surface, which largely determined the design of the actuator and fin.

A. Simulated Control Performance

Equation 1 describes the lift force generated by a thin airfoil with a variable angle of attack, α. This approximation holds for $|\alpha| < 15°$.

$$F_{lift} = \frac{1}{2}\rho V^2 2\pi\alpha A_{ref} \tag{1}$$

$\frac{1}{2}\rho V^2$ describes the dynamic pressure of the airflow surrounding the fin, where ρ is the density of the surrounding air, and V is the speed of the airflow. A_{ref} is the area of the fin in question. As Equation 1 shows, altering the angle of attack of the control surface allows us to linearly control the aerodynamic lift force generated by the surface. In order to remain effective, the control surface must be able generate enough torque to resist this lift force and maintain its angle of attack. Consequently, we must design our control surfaces to meet this torque requirement.

The aerodynamic lift force generated by the control surface applies a torque to the rocket. This provides us with a method of controlling the pitch, roll, and yaw of the rocket. For the pitch and yaw axes, this moment is described by Equation 2. In this equation, d_{cp} is the distance between the control surface and the center of gravity of the rocket. For the roll axis, the torque is described by Equation 3, where r is the radius of the rocket and r_{cp} is the distance from the base of the fin to the center of pressure of the fin.

$$M_{y,z} = F_{lift} d_{cp} \tag{2}$$

$$M_x = F_{lift}(r + r_{cp}) \tag{3}$$

This moment induces a rolling acceleration that alters the rocket's trajectory. The magnitude of this acceleration is determined by the inertial tensor of the rocket, which can be approximated by the inertial tensor of a cylinder (Equation 4).

$$I = \begin{bmatrix} \frac{1}{12}mh^2 + \frac{1}{4}mr^2 & 0 & 0 \\ 0 & \frac{1}{12}mh^2 + \frac{1}{4}mr^2 & 0 \\ 0 & 0 & \frac{1}{2}mr^2 \end{bmatrix} \tag{4}$$

In this expression, m is the mass of the cylinder. Assuming that m scales with S^3, where S represents a single dimension, we find that I scales with S^5. Compared to the control surface force, which scales with S^2, I scales very favorably when size is decreased, which allows us to scale down these rockets

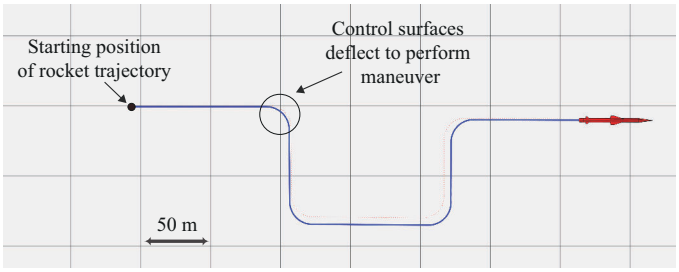

Fig. 2. Simulated trajectory of a millimeter-scale rocket powered by a 5 mN thrust and controlled by MEMS control surfaces. The simulated rocket travelled almost 400 m at a speed of 20 m/s and demonstrated a turning radius of approximately 20 m.

while actually gaining maneuverability. In order to illustrate the MEMS control surfaces' potential utility, we simulated the trajectory of a 3 mm x 6 cm rocket with 5 mN thrust and controlled by MEMS control surfaces. Our simulations show that the rocket is able to perform 18m radius turns at 20 m/s when the control surfaces were generating 5 mN of lift per surface (Figure 2). These simulations show that 5 mN aerodynamic forces are sufficient for controlling the trajectory of a millimeter-scale rocket. This analysis shows us that we can obtain useful maneuverability from just millinewton-scale aerodynamic forces. Fortunately, electrostatic inchworms can easily meet these force requirements, as they have force densities of on the order of $1\frac{\text{mN}}{\text{mm}^2}$ [11].

B. Actuator Design and Fabrication

In our MEMS control surface, electrostatic inchworm motors actuate a rotary slot mechanism that includes a large slotted arm. A 2x4 mm^2 SOI fin is inserted post-fabrication into this slotted arm. Figure 3 shows the layout of the inchworm motors and rotary slot mechanism, which is fabricated in a SOI process. Two inchworm motor arrays are used to to achieve bidirectional rotation; as one motor actuates the other relaxes and allows the shuttle to pass freely through it. The rotary slot mechanism uses silicon pin joints [15] to translate the linear actuation of the inchworm motors to a rotation in the fin slot arm. Additionally, the rotary slot mechanism provides mechanical advantage for the system, so geometric changes in the layout can be made to accommodate different design specifications. The mechanical advantage for our mechanism is $\frac{d_{arm}}{d_p} = 1.36$; d_{arm} is the length of the arm linking the inchworm shuttle to the slotted arm, and d_p is the distance between the slot's fulcrum and the center of pressure of the inserted fin.

As this fin is 40 μm thick and the maximum angle of attack of the actuator is less than 15°, Equation 1 accurately models our control surface. Using calculations from [11], the inchworm motors should have a theoretical force density of $2.11\ \frac{\text{mN}}{\text{mm}^2}$ while running at 110V, which yields 2 mN maximum output force for each 1 mm^2 inchworm motor. We designed this control surface to have a maximum angle of attack of approximately $\pm 10°$ and a maximum output torque of 6 μNm. This output torque corresponds to an output force of 5 mN at

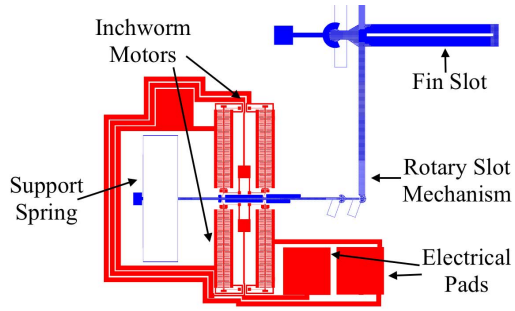

Fig. 3. Layout view of the bottom half of the MEMS control surface chiplet showing inchworm motors in red and the rotary slot mechanism in blue. The top inchworm motor is symmetric with the bottom one. The control surface chiplet is 7 x 9 mm^2.

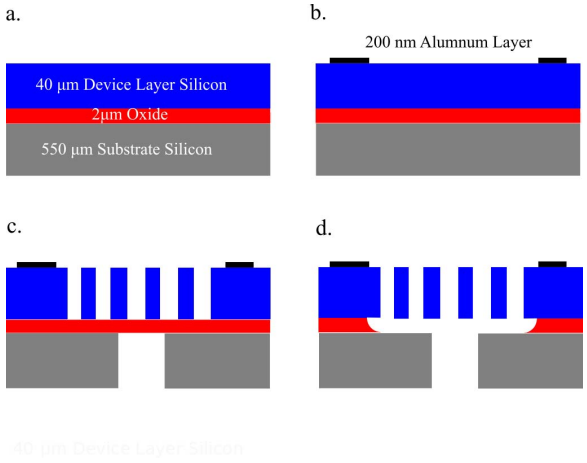

Fig. 4. SOI fabrication process. (a.) SOI wafer before processing. (b.) SOI wafer after evaporation deposition of 200 nm aluminum pads. (c.) Deep reactive ion etch (DRIE) patterns inchworm motors and pin joints in device layer silicon and a backside DRIE etches trenches in the silicon substrate (c.) Hydroflouric acid vapor etch releases device layer structures from the oxide layer.

the fin's center of pressure, which is located at $\frac{1}{4}$ the length fin's chord length. Consequently, this fin should be able to handle a 5 mN aerodynamic lift force while maintaining its angle of attack, which is necessary for the control surface to remain effective.

We fabricated the MEMS control surfaces in a SOI wafer using a lithographic process. The SOI fabrication process is illustrated in Fig. 4. Additionally, we evaporation-deposited a 200 nm layer of aluminum in order to metalize the pads for wirebonding. After fabrication, we assembled the fin structure by inserting the fin into the fin slot and securing it with silver epoxy. We then mounted the structure on a flex-printed circuit board (PCB) and wirebonded the PCB pads to the metalized control surface pads. Figure 5 shows the fully assembled control surface system. External wires were soldered to the PCB pads and used as power lines for the inchworm motors.

III. Method

We performed both functionality and force characterization experiments for the control surfaces. Displacement angles of the fin slot were determined visually by capturing images with

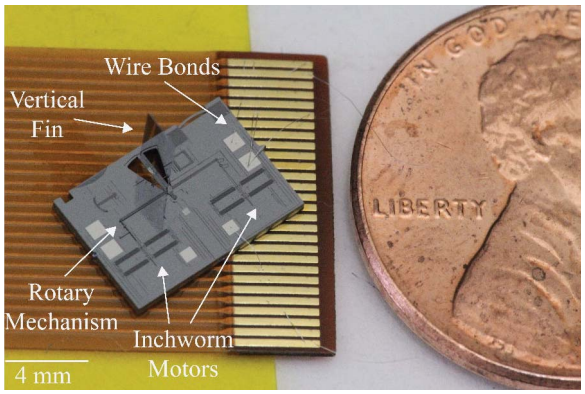

Fig. 5. Fully assembled and wirebonded fin. The total size of this assembly is 7 mm x 9 mm x 3 mm.

a microscope camera and measuring the angular displacement using digital image editing software. We designed force gauge test structures attached to the fin slot to aid the characterization of the force output (see Figure 7). This test structure is attached to the same position on the fin slot as where the center of pressure of the inserted fin would be located, so the force applied by the force gauge should map equivalently to an aerodynamic lift force generated by the fin. In order to measure the output force of the fully assembled control surface, we placed a mounted needle on a scale and rested the fin on the needle. We then actuated the fin and measured the change in weight on the scale. We used an Arduino Uno with high voltage MOSFETs to generate the necessary inchworm motor control signals from a 0-120V DC power supply.

IV. Results

We were able to achieve maximum deflections of 10° in the fin slot while operating an unassembled control surface at a probe station. Figure 6 illustrates this actuation. The maximum speed these inchworm motors could be run before failing to actuate was 3.5 kHz. This limit on drive frequency is most likely due to the RC time constant of the motor capacitance and the pull up resistors in the switching circuit. We could likely increase the maximum motor frequency by using more sophisticated switching circuits that would reduce the RC constant.

Additionally, we estimated the force output of actuator mechanism using our force gauge test structure. Force outputs were estimated by first measuring the angular displacement of the fin slot. We then derived the spring constant of the force gauge from its layout dimensions and used it to convert the displacement of the fin slot into a force. Results of this experiment are shown in Figure 7. The maximum estimated output force was 1.5 mN, which was reached at 80V. At 80V, the actuator reached its maximum deflection point, which saturated the measurement from the force gauge. Interestingly, the estimated actuator force was not quadratically related to voltage, which is how theoretical electrostatic actuators normally behave. This phenomenon could be explained by an increased electrostatic attraction between the substrate and a released rotary slot mechanism that are at different voltages. While these structures are both designed to be at the same ground potential, they could easily develop a voltage differen-

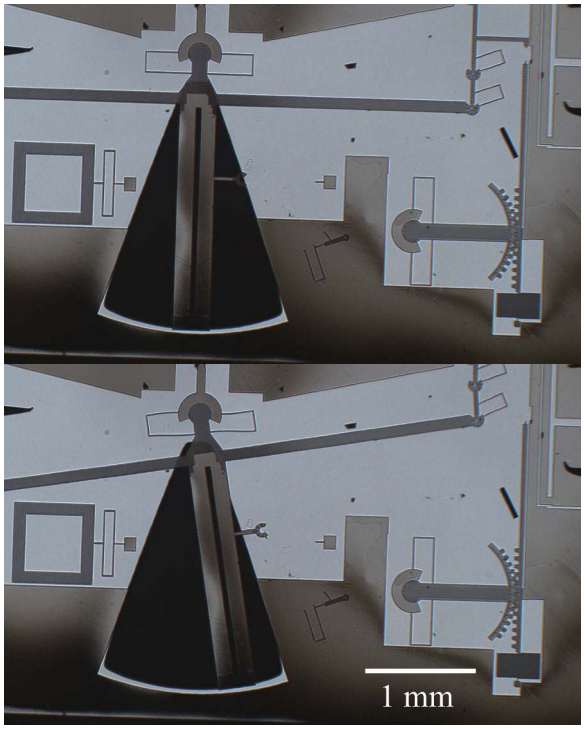

Fig. 6. Top: Rotary slot mechanism at no deflection. Bottom: Mechanism at maximum deflection of 10°. This motor was being driven at 90V and a frequency of 100Hz.

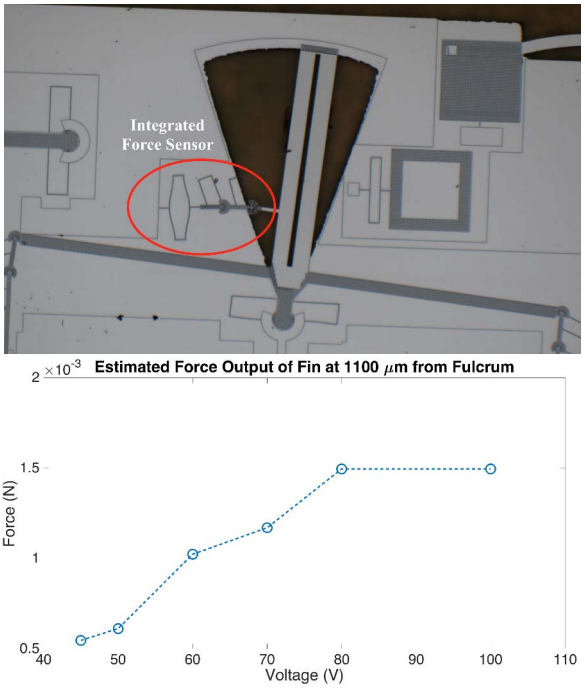

Fig. 7. Top: Integrated force gauge experiment used for estimating output force of control surface. Bottom: Estimated force vs. voltage plot for the MEMS control surface. We optically measured the displacement of the force gauge and calculated the applied force by using the simulated spring constant of the structure.

tial if small conductive debris, such as silicon shards, create a weak electrical connection between an electrical drive trace and another structure.

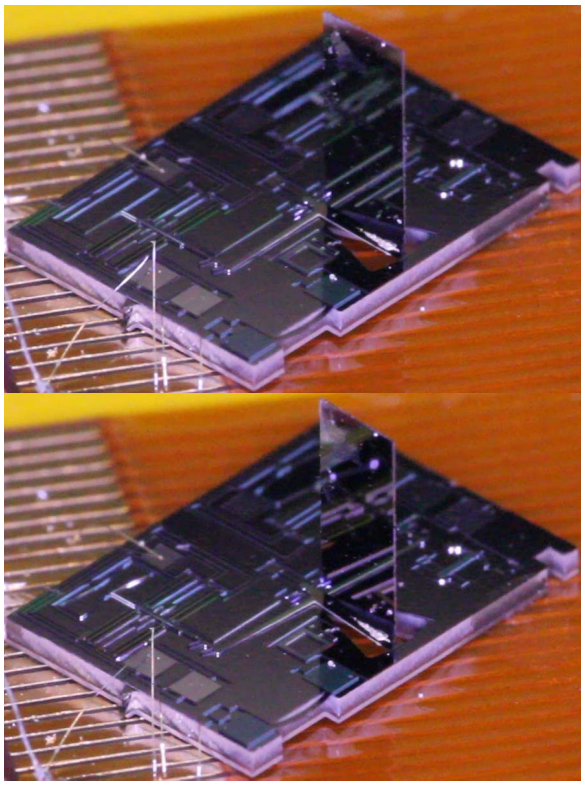

Fig. 8. Demonstration of fully assembled fin actuating. Top: Fin at rest. Bottom: Fin at a deflection of 5°.

We also demonstrated the successful actuation of the fully-assembled control surface (see Figure 8). The assembly allowed us to drive the control surface outside of a probe station, which is necessary for independent operation on an miniature aerial vehicle like a millimeter-scale rocket.

Finally, we characterized the force output of the fully assembled control surface (see Figure 10. The maximum measured force was 1.05 mN at a distance of 1500 μm from the fulcrum, which corresponds to a maximum torque of 1.575 μNm. The measured output force of the fully-assembled control surface is similar to the measured output force measured by the integrated silicon force gauge when differences in mechanical advantage are taken into account. Additionally, the output force of the fully-assembled control surface is not quadratically dependent on input voltage. At a maximum output torque of 1.575 μNm, the assembled control surface performs at 26.3% of its expected performance. This could be attributed to stiction, friction, and parasitics in the structure. We can address this performance discrepancy in future designs by increasing the mechanical advantage of the rotary slot mechanism or increasing the inchworm motor area to increase torque.

V. Conclusion

This work demonstrates the design, fabrication, and assembly of MEMS aerodynamic control surfaces. Our control surfaces utilized high force density and displacement inchworm motors along with planar silicon pin joints to rotationally deflect a silicon fin. We determined what forces are required to effectively maneuver a millimeter-scale rocket with control

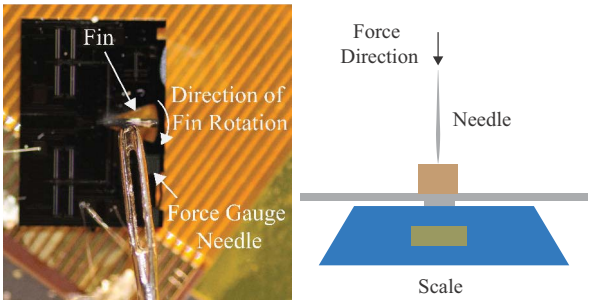

Fig. 9. Left: Force gauge tip placed underneath the fin. This needle was oriented vertically and the fin would rotate down into it. As the fin actuated downward, it pressed down on the needle, and the resulting force was measured by a scale below. Right: Illustration of needle-scale force gauge.

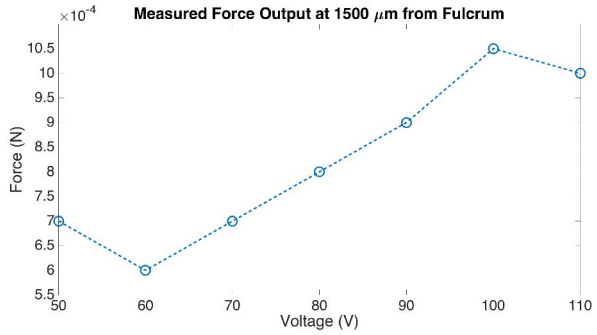

Fig. 10. Measured force vs. voltage plot of the fully-assembled control surface. The inchworm motors were operating at a frequency of 500 Hz when this data was taken.

surfaces through simulation. Our force characterization of the control surfaces found that they indeed generate useful amounts of force for MAVs like millimeter-scale rockets. The maximum output torque of the control surface was measured to be 1.575 μNm, which is enough to sustain an aerodynamic lift force of 1.4 mN on the fin. Future work will focus on characterizing the aerodynamic lift the MEMS control surface can generate and integrating the control surface into a standalone millimeter-scale electronic control system. Ultimately, we plan to demonstrate controlled flight of millimeter-scale rockets and centimeter-scale jet aircraft [6] using multiple MEMS control surfaces.

Acknowledgments

We would like to thank the UC Berkeley Marvell Nanofabrication Facility for the use of their facilities, which made this research possible.

References

[1] D. Hambling, *Swarm Troopers: How small drones will conquer the world*. Archangel Ink, 2015.

[2] N. Stephenson, *The Diamond Age*. Bantam, 1995.

[3] W. Lindsay, D. Teasdale, V. Milanovic, K. Pister, and C. Fernandez-Pello, "Thrust and electrical power from solid propellant microrockets," in *MEMS*, 2001.

[4] M. Kovac, M. Bendana, R. Krishnan, J. Burton, M. Smith, and R. J. Wood, "Multi-stage micro rockets for robotic insects," *Robotics: Science and Systems VIII*, p. 185, 2013.

[5] R. J. Wood, B. Finio, M. Karpelson, K. Ma, N. O. Pérez-Arancibia, P. S. Sreetharan, H. Tanaka, and J. P. Whitney, "Progress on picoair vehicles," *The International Journal of Robotics Research*, vol. 31, no. 11, pp. 1292–1302, 2012.

[6] D. Drew, B. Kilberg, and K. Pister, "Future mesh-networked pico air vehicles," in *Intl. Conf. Unmanned Aircraft Systems*, 2017.

[7] C.-M. Ho and Y.-C. Tai, "Micro-electro-mechanical-systems (mems) and fluid flows," *Annual Review of Fluid Mechanics*, vol. 30, no. 1, pp. 579–612, 1998.

[8] A. L. Murthy and Y. Krishna, "Design and analysis of mems-based microballoon actuators for aerodynamic control of flight vehicles," *Defence Science Journal*, vol. 59, no. 6, p. 642, 2009.

[9] S. E. Lyshevski, "Smart flight control surfaces with microelectromechanical systems," *IEEE Transactions on Aerospace and Electronic Systems*, vol. 38, no. 2, pp. 543–552, 2002.

[10] R. Low, M. Deeds, D. Jean, and C. Hovland, "Mems control surface for projectile steering," Dec. 8 2009, uS Patent 7,628,352. [Online]. Available: https://www.google.com/patents/US7628352

[11] I. Penskiy and S. Bergbreiter, "Optimized electrostatic inchworm motors," *J. Micromech. Microeng.*, vol. 23, 2013.

[12] R. Yeh, S. Hollar, and K. S. Pister, "Single mask, large force, and large displacement electrostatic linear inchworm motors," *Journal of Microelectromechanical Systems*, vol. 11, no. 4, pp. 330–336, 2002.

[13] D. S. Contreras, D. Drew, and P. K. S. J., "First steps of a millimeter-scale walking silicon robot," in *Solid State Sensors, Actuators, and Microsystems*, 2017, in press.

[14] S. Hollar, a. Flynn, C. Bellew, and K. Pister, "Solar powered 10 mg silicon robot," *The Sixteenth Annual International Conference on Micro Electro Mechanical Systems, 2003. MEMS-03 Kyoto. IEEE*, pp. 706–711, 2003.

[15] D. S. Contreras and K. S. J. Pister, "Durability of Silicon Pin-Joints for Microrobotics," in *MARSS*, 2016.